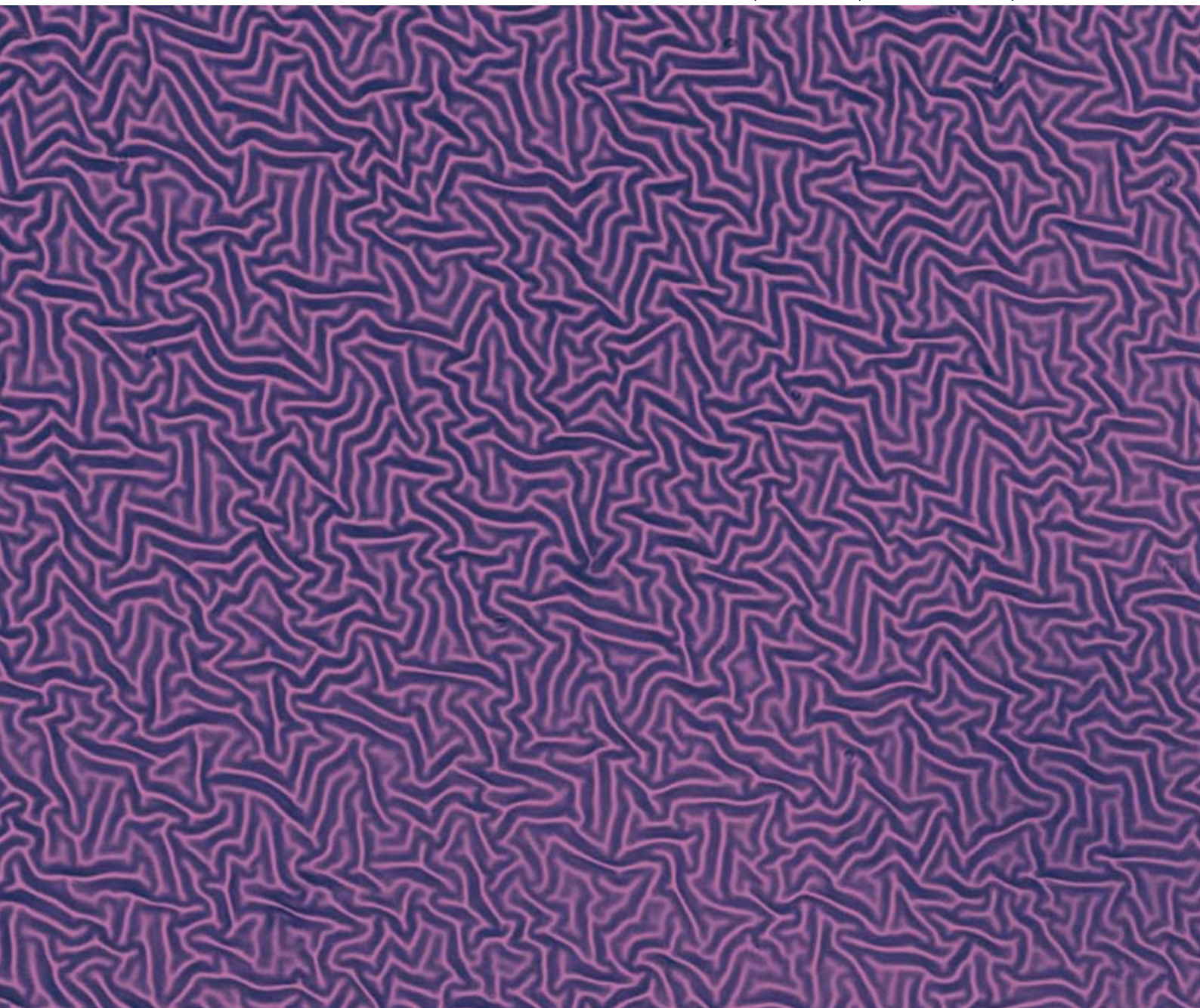


Soft Matter

www.softmatter.org

Volume 4 | Number 12 | 1 December 2008 | Pages 2285–2528



ISSN 1744-683X

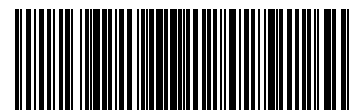
RSC Publishing

COMMUNICATION

João T. Cabral *et al.*
Complex micropatterning of periodic
structures on elastomeric surfaces

HIGHLIGHT

Joel H. Collier
Modular self-assembling biomaterials
for directing cellular responses



1744-683X(2008)4:12;1-A

Complex micropatterning of periodic structures on elastomeric surfaces†‡

Arnaud Chiche,[§] Christopher M. Stafford^a and João T. Cabral^{*b}

Received 10th July 2008, Accepted 15th August 2008

First published as an Advance Article on the web 30th September 2008

DOI: 10.1039/b811817e

We report a simple methodology to fabricate complex sub-micrometre periodic structures in poly(dimethylsiloxane) over large surface areas (several cm²). Single-frequency, uni- and multi-axial sinusoidal surface modulations, with tunable amplitude and wavelength, in the nano- to micrometre range, are readily demonstrated. The technique builds upon a buckling instability of a stiff layer supported by an elastomeric membrane (reported earlier), induced by surface oxidation of a pre-stretched elastomer coupon followed by removal of the applied mechanical strain. Plasma oxidation yields model surfaces with single wavelengths, sub-micrometre periodicity, achieving a dynamic range from sub-200 nm to 10s of μm , which UV ozonolysis extends to 100s of μm . We find that a single ‘dose’ parameter (exposure time \times power) characterizes the surface conversion. The strain control provides unprecedented tunability of surface pattern amplitude and morphology, ranging from lines to complex periodic topologies induced under multi-axial deformation. We introduce a novel multiple strain–exposure and replication approach that extends surface topologies beyond lines, chevron and spinodal patterns (isotropic structures with a dominant wavelength). The resulting structures exhibit a glass-like surface, which is easily grafted with self-assembled monolayers to enhance functionality. Applications of this inexpensive and fast methodology include stamps for soft lithography, micromolding, templating and surface patterning.

Patterning of soft materials provides an exceptional route for the generation of nano- to microstructured and functional surfaces. Non-photolithographic methods are attractive due to their simplicity and low cost but also because of their versatility, surface 3-dimensionality and varied surface chemistry.¹ Applications range from organic electronics^{2,3} to bio-patterning.⁴ Soft lithography techniques include microcontact printing, stamping, templating, and micromolding, and typically involve transferring patterns *via* an elastomeric material. Poly(dimethylsiloxane), PDMS, provides high fidelity replication, optical transparency, widely suitable surfaces and adhesive properties for patterning, and thus has become ubiquitous in soft

lithography. The ability to generate self-organized surface patterns that span from nano- to microscale in a simple and rapid fashion remains however a challenge. For this purpose, we introduce an effortless approach, coupling controlled straining and simultaneous surface oxidation of an elastomeric membrane that is capable of generating large area, model sub-micrometre periodic surfaces with fine dimensional control.

We exploit a well-known buckling instability of stiff supported layers under compression,^{5,6} with implications that range from the stability of macroscopic sandwich-panel structures (*e.g.* aircraft wings)^{7,8} to microscopic wrinkling of biological membranes.⁹ Assuming perfect adhesion of the top stiff layer with a much thicker soft elastic substrate (no slippage or delamination), the uni-axial compression of this bilayer results in a sinusoidal buckling, whose wavelength λ and amplitude A are given by^{8,10–13}

$$\lambda(E_s, E_f, h_f) = 2\pi h_f \left(\frac{\bar{E}_f}{3E_s} \right)^{1/3} \quad (1)$$

$$A(E_s, E_f, h_f, \varepsilon) = h_f \left(\frac{\varepsilon}{\varepsilon_c} - 1 \right)^{1/2} \quad (2)$$

where $\bar{E} = E/(1 - \nu^2)$ is the plane-strain modulus, h_f is the top film thickness, E the Young’s modulus, ν the Poisson’s ratio (material compressibility) and ε the compressive strain applied to the bilayer. Indices f and s refer to, respectively, the supported film and the soft substrate. Note that only the amplitude, but not the wavelength, depends on the strain,¹⁴ provided that a threshold value for buckling

$$\varepsilon_c = -\frac{1}{4} \left(\frac{3\bar{E}_s}{\bar{E}_f} \right)^{2/3} \quad (3)$$

is exceeded.^{11,12} Both amplitude and wavelength are directly proportional to the thickness of the top film h_f which is the leading parameter of eqn (1) and (2).

Applications of this surface instability in materials science have been recently reported, including mechanical testing of thin films,¹⁵ tunable optical phase gratings¹⁶ and microchannel filtration.¹⁷ Micropatterning using surface buckling has also been demonstrated,^{15,17–20} using various stiff materials deposited onto PDMS. In order to minimize film delamination and cracking, the deposition of top layers onto pre-strained PDMS, followed by strain relaxation, is desirable for patterning applications. Whitesides and co-workers reported that metal evaporation of a thin film onto thermally expanded and oxidized PDMS results in a (spinodal-like) isotropic surface undulation in the micrometre-range upon contraction induced by cooling. Additional surface complexity was reached by partially masking the surface during metallization.¹⁹ Oriented patterns with dominant wavelengths of 10s of micrometres have been achieved by the oxidation of a pre-strained silicone rubber surface by

^aPolymers Division, National Institute of Standards and Technology, MD 20899, USA

^bDepartment of Chemical Engineering, Imperial College London, London, UK SW7 2AZ. E-mail: j.cabral@imperial.ac.uk

† Official contribution of the National Institute of Standards and Technology; by acceptance of this article, the publisher and/or recipient acknowledges the US Government’s right to retain a nonexclusive, royalty-free license in and to any copyright covering this paper.

‡ Electronic supplementary information (ESI) available: Comparison between Plasma and UVO oxidation. See DOI: 10.1039/b811817e

§ Present address: DSM Material Science Centre, P.O. Box 18, 6160 MD Geleen, The Netherlands.

UV ozonolysis (UVO), which is then relaxed causing the top layer to buckle. The resulting layer exhibits, however, multiple wavelengths¹⁷ due to the complex structure of the relatively thick (≈ 50 nm) oxide layer.^{21,22}

Conversely, plasma treatment of PDMS produces comparatively extremely thin (≈ 5 nm), stiff and uniform glassy surface layers^{21,23–25} permitting sub-micrometre buckling [*cf.* eqn (1)] while preserving the chemical functionality of the silicates. Plasma surface modification appears therefore ideally suited for surface patterning and sub-micrometre buckling of PDMS membranes, as recently reported by two groups.^{20,26} In their work, ‘pre-straining’ was caused by thermal expansion induced during plasma treatment, thus resulting in isotropic patterns similar to those obtained with metalized surfaces^{18,27} discussed above. Further, despite the large coefficient of thermal expansion of crosslinked PDMS ($\approx 3.1 \times 10^{-6} \text{ K}^{-1}$) in comparison to silicon or glass ($1 \times 10^{-6} \text{ K}^{-1}$ to $1 \times 10^{-7} \text{ K}^{-1}$) the effective plasma temperature of $200 \text{ }^\circ\text{C}$ to $300 \text{ }^\circ\text{C}$ results in strains of $\sim 1\%$.²⁰ Mechanical strain opens the door to higher applied strains (10–50%) and thus larger amplitudes, as well as controlled multi-axial topologies.

We now explore a combined oxidation treatment (plasma or UVO) with prescribed, directional pre-straining in order to pattern sub-micrometre model surfaces with controlled morphologies. Each experimental step, depicted in Fig. 1, is rather straightforward. It involves (a) casting an elastomeric silicone sheet, which is (b) stretched under controlled strain, followed by surface treatment and (c) relaxed to trigger the surface undulations. Pre-straining of the PDMS prior to oxidation offers several advantages over compressing the bilayer after treatment. Compression of the elastomer membrane results inevitably in bending²⁸ and therefore in a curved patterned surface; additionally, such compression must be applied constantly to maintain the wrinkled surface pattern for subsequent use. In contrast, a pre-strained elastomeric coupon, once relaxed, yields a flat, stable, patterned surface. Alternatively, uni-axial stretching of a (nearly

incompressible) rubber can also lead to compression in the orthogonal direction (Poisson’s effect) and therefore buckling.¹⁵ However, the large tensile deformation results in cracking of the brittle oxide layer orthogonal to the stretching direction,²⁹ while buckling becomes a secondary effect as the lateral compressive strain is significantly lower than the applied tensile strain (approximately 8% compression strain for 20% tensile strain). In contrast, buckling is the dominant effect in pre-strained surfaces, directly generated by controlling the applied strain.

PDMS (Sylgard 184, Dow Corning, 10 : 1 by mass base to crosslinker) sheets of 3 mm thickness were cast onto flat glass plates, degassed and cured overnight at ambient condition. The PDMS was then thermally cured at $75 \text{ }^\circ\text{C}$ for 2 h. Typically, rectangular specimens of $5 \text{ cm} \times 1 \text{ cm}$ were cut with a razor blade and mounted onto a strain stage. Uni-axial strain was first induced by clamping the sample extremities and stretching along the long dimension, typically from 0 to 40%, using a simple setup described elsewhere.³⁰ More complex planar strains resulting in higher order structures were generated using other setups, including an inflated membrane or a folded sheet, which we describe below. Surface treatment was carried by oxygen plasma oxidation (Anatech SP-100, VA) with prescribed power (from 10 W to 100 W) and exposure time (from 15 s to 20 min). Alternatively, UVO treatment was carried out using a Jelight 342 cleaner, placing the specimen 3 mm away from the light source and using exposure times from 10 min to 1 h. By varying the treatment parameters, namely exposure time and power, we can tune the oxide layer thickness and modulus and thus directly control the pattern wavelength. The crosslinked PDMS has a modulus of ~ 1.5 MPa³¹ and Poisson ratio of 0.48–0.50, while we estimate that the glass-like oxidized layer has a modulus of ~ 40 GPa and much lower Poisson ratio (0.17 for pure silica and modulus of 70 GPa). Surface characterization was carried out by optical and atomic force microscopy (Veeco Dimension 3000) as well as stylus profilometry (Dektak 8).³²

As illustrated in Fig. 1, regular patterns are easily produced (here with lines orthogonal to the uni-axial pre-strain), with wavelengths ranging from below 200 nm up to several micrometres, using oxygen plasma. In comparison, UVO treatments generate a main wavelength ranging from few to hundreds of micrometres, and multiple buckles at lower scales are observed [ESI†], in accord with previous reports.¹⁷ The complementarity of length scales derives from both the nature of the oxidation process and the accessible thickness (h_i) of the oxidized layer *via* both techniques, discussed below.

The control of the pattern is typically two fold: by controlling the exposure dose, the wavelength is directly tuned. Then for a given wavelength, the amplitude is separately tuned by the applied strain, up to approximately $A \approx 30\%$ of the wavelength value (Fig. 2b). The limitation on the amplitude arises from the fact that large strains result in deformations that are no longer sinusoidal. Indeed the buckling instability model employed [eqn (1) and (2)] is only applicable to small deformations. Fig. 2a presents the variation of both wavelength and amplitude with the plasma exposure dose, for a fixed initial strain of $\varepsilon = 20\%$. We find that experimental results of λ and A superpose for various combinations of exposure *time* and *power*, as shown in Fig. 2. We therefore conclude that a single parameter, the plasma dose, defined as $dose[J] = time \times power$ (at constant oxygen pressure $p = 50$ Pa) describes all data. Very high dose treatments have been realized by successive exposures at limited doses (typically up to 10 kJ) in order to avoid significant warming of the sample and its

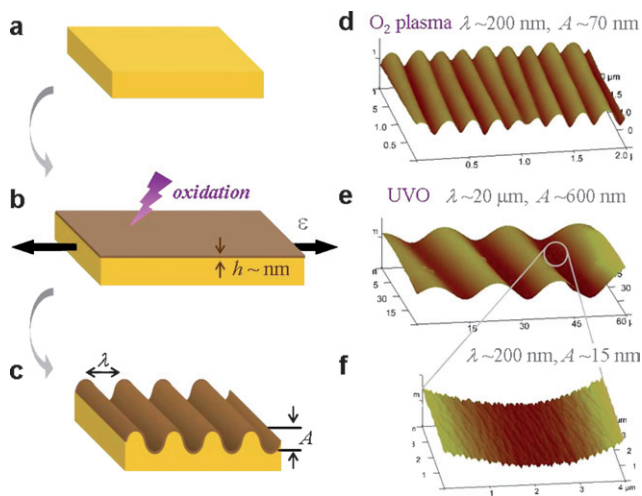


Fig. 1 Uni-axial patterning step: (a) a crosslinked PDMS slab is (b) uni-axially deformed and held stretched during oxygen plasma exposure, and (c) the surface buckles upon strain release after the treatment. (d–f) Permanent, crack-free, model patterned surfaces are obtained (AFM micrographs). Sinusoidal patterns with wavelengths ranging from 100 nm to 100 μm are defined by the oxidation treatment, either *via* plasma or UVO, and exposure dose [see ESI†].

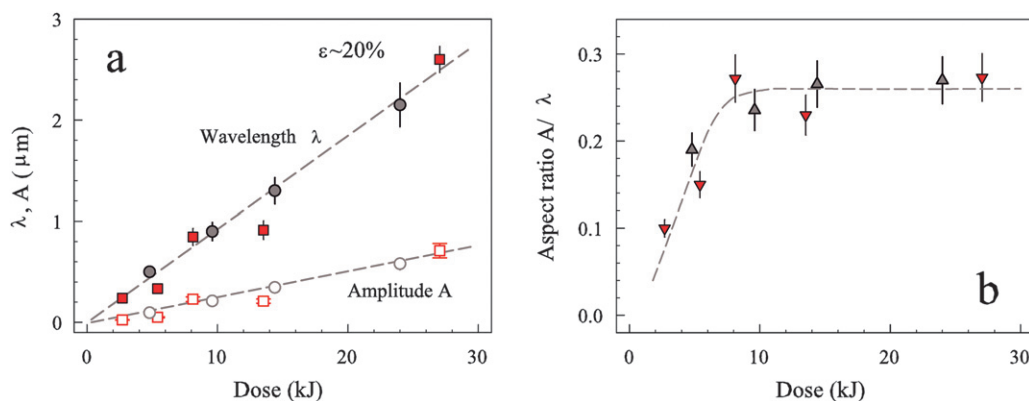


Fig. 2 (a) Amplitude (A) and wavelength (λ) of surface patterns generated by oxygen plasma exposure at constant strain (20% shown here). The dose (power \times time) can be either controlled by exposure time (\blacksquare , \square at constant power of 80 W) or power (\bullet , \circ time = 5 min). (b) The pattern aspect ratio A/λ increases with the dose (\blacktriangledown power 80 W, \blacktriangle time = 5 min) until reaching a plateau for doses higher than ~ 10 kJ. Dashed lines are guides to the eye. The error bars represent one standard deviation of the data, which is taken as the experimental uncertainty of the measurement.

subsequent thermal expansion. The dose superposition and cumulative nature of the oxidation process provides access to a wide dynamic range of A and λ *via* tuning the oxide layer thickness h_f .

To the best of our knowledge, this is the first quantitative report of the amplitude of such a buckling pattern. Rather unexpectedly, we find that the wavelength and the amplitude exhibit the same dependence with dose. This dependence is linear within the range investigated here but eventually becomes logarithmic for large doses.³³ As shown in Fig. 2b, this corresponds to an aspect ratio amplitude/wavelength *independent* from the treatment dose, for values in excess of 10 kJ.

According to eqn (1) and (2), the aspect ratio of the surface pattern of a layer of modulus \bar{E}_f can be written as

$$\frac{A}{\lambda} = \frac{1}{\pi}(\Delta\varepsilon)^{1/2} \quad (4)$$

where $\Delta\varepsilon \equiv \varepsilon - \varepsilon_c$. A plateau of the aspect ratio is expected if the modulus of the oxide layer \bar{E}_f is not affected by the dose, the ratio being controlled solely by the strain as in eqn (4). Our results indicate that increasing the plasma treatment exposure above a certain value does *not* affect the modulus of the oxide layer generated but only its thickness, which in the range shown here increases linearly with the dose. A detailed study of the wave-like propagation of the oxidized layer (orthogonal to the surface) induced by plasma exposure is currently underway.

For exposure doses *below* the threshold of 10 kJ however, the aspect ratio increases with the dose, *via* the critical threshold ε_c , which depends on \bar{E}_f [according to eqn (3)]. This indicates a correspondence between the treatment dose and the modulus \bar{E}_f of the oxidized layer, and we interpret this increase as a build-up of the glass-like layer. As oxidation proceeds, the density of the top layer increases from pure silicone elastomer to the final value of the oxidized layer. The latter is constant, as shown by the plateau in aspect ratio. This increase is accompanied by an increase in both the stiffness of the oxide layer and the resulting pattern aspect ratio. For very low dose treatments, the conversion and thus the density and stiffness of the oxide layer are low and a broad ‘unsaturated’ conversion profile forms orthogonal to the sample surface. The single supported layer assumption is no longer valid, and interferences between the multiple wavelengths generated by such a profile create irregular patterns with micrometre

wavelengths or larger. This directly limits the wavelength accessible with this patterning technique for a given elastomer.

The patterns reported above consist of sinusoidal waves induced by uni-axial strain. However, the shape and complexity of the patterns accessible with this method depend directly on the strain field used to generate the local compression of the supported layer after plasma exposure. Fig. 3 presents illustrative patterns we could readily produce with simple multi-axial strain fields. A schematic of the strain field associated with each pattern is shown. Patterns a and b have been produced in a single exposure. The isotropic strain in Fig. 3a was generated by inflating a thinner (500 μm) elastomer membrane held in a ring, deformed like a balloon. This method allows much higher strains (more than $\varepsilon \approx 30\%$) than by thermal expansion as reported

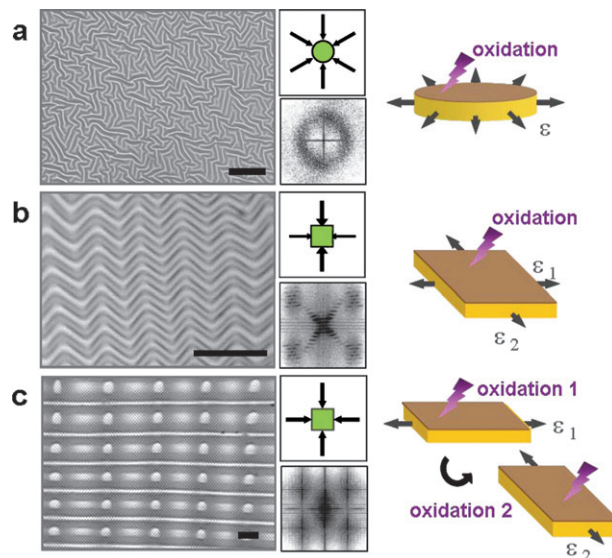


Fig. 3 Optical micrographs and FFT of surface patterns generated by single and multi-axial strain fields (indicated by schematics) coupled with plasma (a,b) or UVO (c) exposure. Patterns (a,b) are generated by a single exposure step and yield isotropic and chevron topologies (in addition to lines in Fig. 1a). Pattern (c) yields a checkerboard pattern consisting of peaks and saddles, which has been produced by two successive exposure–strain steps. Scale bars are 20 μm .

previously,^{18,19,27} and therefore results in higher aspect ratios (up to 30% compared to few percent). The chevron (or herringbone) pattern in Fig. 3b was obtained by folding a thick (10 mm) PDMS slab onto itself. Due to its incompressibility, the slab curves outwards at the edges resulting in a horse saddle shape. The main folding induces the principal compressive strain component while the lateral bending induces the minor component and creates chevrons. Recently Lin and Yang³⁴ also demonstrated the reversible formation of chevron patterns of 500 nm to 2.5 μm using thin membranes. In contrast, the pattern in Fig. 3c results from two successive uni-axial UVO patterning steps (*cf.* Fig. 1) in orthogonal directions, resulting in an interference pattern yielding a rectangular network of peaks and saddles.

To produce patterns through multiple exposures, one needs to replicate the pattern with PDMS between each strain–exposure and use this unoxidized slab to avoid stretching of the supported glass layers, which otherwise causes cracking of the surface pattern, limiting its usable surface. Further, the replication step allows the build-up of a new oxidized layer of prescribed thickness and an additional buckling step, extending the range of topologies accessible well beyond lines, chevron or isotropic structures. Octadecylsiloxane (ODS) is evaporated overnight under vacuum on the surface, then rinsed with ethanol and dried, in order to release the patterned replica from the master. It is necessary to perform the second exposure on a PDMS replica of the first pattern, as shown in Fig. 4, illustrated for a pattern produced by two orthogonally-stretched UVO exposures. The accessible patterns are defined by four decoupled parameters, namely two wavelengths (λ_1 , λ_2) and two amplitudes (A_1 , A_2) determined *separately* by exposure (plasma, UVO) dose and strain, and finally by strain geometry (or relative angle for uni-axial strain shown here). These results generally demonstrate that a variety of model periodic surface patterns can be readily generated, with dimensions tuned by accessible experimental parameters, resulting from the interference of surface buckling waves. The complex interplay between the surface waves (*e.g.*, mismatch between λ and A) clearly opens novel patterning avenues which are currently under study.

In summary, we report a simple and comparatively inexpensive sub-micrometre patterning technique, capable of generating controlled and regular patterns with wavelengths from below 200 nm up to several micrometres and amplitudes up to 30% of the wavelength for a given strain ($\epsilon = 20\%$). Smaller wavelengths, *circa* 100 nm and below, should be accessible by the use of stiffer elastomers than PDMS (highly crosslinked or filled),³¹ according to eqn (1). We find

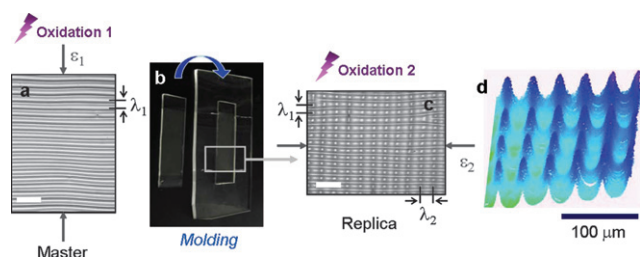


Fig. 4 Multiple strain–oxidation and replication approach, depicting (a) the pattern obtained after uni-axial strain–exposure, (b) replication onto PDMS after ODS grafting, (c) the 2D structure after the second strain–exposure step (orthogonal shown here). (d) A stylus profilometry scan of the rectangular arrays of peaks and saddles generated by this versatile double exposure (scale bar 100 μm).

that the ‘dose’ is the governing parameter for the oxidation process. Complex hierarchical patterns beyond lines, chevron and isotropic topographies are demonstrated for the first time, introduced by a simple multiple strain–exposure approach. Compared to established lithography techniques, our method is restricted to single, superposed sinusoids and interference surface patterns with sub-micrometre to micrometre dimensions. However, this approach has the great advantage of simplicity, rapidity and low cost as surface patterns are generated within minutes using readily available elastomer rubbers. Unlike other methods based on a buckling instability previously reported, we demonstrate regular and controlled patterns, both in shape and dimensions (separately A and λ), crack-free over large areas and with sub-micrometre wavelengths. The complementarity of length scales accessible *via* plasma and UVO oxidation are established from sub-200 nm (plasma) to 100s of μm (UVO), arising from the nature of the oxidized surface formed. The pattern surface chemistry, analogous to glass, is amenable to direct transformations, including grafting, bonding/sealing, templating or transfer. Further, the resulting sinusoidal shape of the patterns (challenging to achieve *via* lithography) can be subsequently converted into a square wave (with sharp edges) *via* pattern transfer or nanoimprint. The resulting surface topologies are readily replicated or used as sub-micrometre microfluidic photomasks for lithography, by filling the surface channels with absorbing ink *via* capillarity. Such a versatile approach permits any group to directly and inexpensively (requiring no master fabrication) access sub-micrometre patterning for a plethora of soft matter applications, including stamping, micromolding and templating.

Notes and references

- 1 Y. Xia and G. M. Whitesides, *Angew. Chem., Int. Ed.*, 1998, **37**, 550.
- 2 D.-Y. Khang, H. Jiang, Y. Huang and J. A. Rogers, *Science*, 2006, **311**, 208.
- 3 M. Cavallini, P. Stolar, J.-F. Moulin, M. Surin, P. Leclère, R. Lazzaroni, D. W. Breiby, J. W. Andreasen, M. M. Nielsen, P. Sonar, A. C. Grimsdale, K. Mullen and F. Biscarini, *Nano Lett.*, 2005, **5**, 2422.
- 4 D. B. Weibell, W. R. DiLuzio and G. M. Whitesides, *Nat. Rev. Microbiol.*, 2007, **5**, 209.
- 5 J. Genzer and J. Groenewold, *Soft Mater*, 2006, **2**, 310.
- 6 J. Groenewold, *Physica A*, 2001, **298**, 32.
- 7 M. A. Biot, *J. Appl. Mech.*, 1937, **4**, A1.
- 8 H. G. Allen, *Analysis and Design of Structural Sandwich Panels*, Pergamon, New York, 1969.
- 9 E. Cerda, K. Ravi-Chandar and L. Mahadevan, *Nature*, 2002, **419**, 579.
- 10 A. L. Volynskii, S. Bazhenov, O. V. Lebedeva and N. F. Bakeev, *J. Mater. Sci.*, 2000, **35**, 547.
- 11 Z. Y. Huang, W. Hong and Z. Suo, *J. Mech. Phys. Solids*, 2005, **53**, 2101.
- 12 R. Huang, *J. Mech. Phys. Solids*, 2005, **53**, 63.
- 13 H. Jiang, D.-Y. Khang, J. Song, Y. Sun, Y. Huang and J. A. Rogers, *Proc. Natl. Acad. Sci. U. S. A.*, 2007, **104**, 15607.
- 14 The wrinkling wavelength λ eventually depends on strain ϵ for large deformations, as indicated by recent experiments and analytical model by Jiang *et al.*¹³. The ‘classical’ model presented here is applicable in the small deformation limit.
- 15 C. M. Stafford, C. Harrison, K. L. Beers, A. Karim, E. J. Amis, M. R. VanLandingham, H.-C. Kim, W. Volksen, R. D. Miller and E. E. Simonyi, *Nat. Mat.*, 2004, **3**, 545.
- 16 C. Harrison, C. M. Stafford, W. Zhang and A. Karim, *Appl. Phys. Lett.*, 2004, **85**, 4016.
- 17 K. Efimenko, M. Rackaitis, E. Manias, A. Vaziri, L. Mahadevan and J. Genzer, *Nat. Mat.*, 2005, **4**, 293.
- 18 N. Bowden, S. Brittain, A. G. Evans, J. W. Hutchinson and G. M. Whitesides, *Nature*, 1998, **383**, 146.

-
- 19 W. T. S. Huck, N. Bowden, P. Onck, T. Pardoën, J. W. Hutchinson and G. M. Whitesides, *Langmuir*, 2000, **16**, 3497.
- 20 D. B. H. Chua, H. T. Ng and S. F. Y. Li, *Appl. Phys. Lett.*, 2000, **76**, 721.
- 21 K. Efimenko, W. E. Wallace and J. Genzer, *J. Colloid Interface Sci.*, 2002, **254**, 306.
- 22 M. Ouyang, C. Yuan, R. J. Muisener, A. Boulares and J. T. Koberstein, *Chem. Mater.*, 2000, **12**, 1591.
- 23 M. J. Owen and P. J. Smith, *J. Adhes. Sci. Technol.*, 1994, **8**, 1063.
- 24 H. Hillborg and U. W. Gedde, *Polymer*, 1991, **39**, 1998.
- 25 H. Hillborg, J. F. Ankner, U. W. Gedde, G. D. Smith, H. K. Yasuda and K. Wikström, *Polymer*, 2000, **41**, 6851.
- 26 A. Tserepi, E. Gogolides, K. Tsougeni, V. Constantoudis and E. S. Valamontes, *J. Appl. Phys.*, 2005, **98**, 113502.
- 27 N. Bowden, W. T. S. Huck, K. E. Paul and G. M. Whitesides, *Appl. Phys. Lett.*, 1999, **75**, 2557.
- 28 L. D. Landau and E. M. Lifshitz, *Theory of Elasticity*, Pergamon, New York, 1986.
- 29 D. Tsubone, T. Hasebe, A. Kamijo and A. Hotta, *Surf. Coat. Technol.*, 2007, **201**, 6423.
- 30 C. M. Stafford, S. Guo, C. Harrison and M. Y. M. Chiang, *Rev. Sci. Instrum.*, 2005, **76**, 062207.
- 31 The modulus of Sylgard changes slowly during crosslinking after 1–2 h and is estimated to increase by 1% between 1 h and 4 h at 65 °C [Y. Zhao and X. Zhang, Mechanical properties evolution of polydimethylsiloxane during crosslinking process, in *Mater. Res. Soc. Symp. Proc.: Mechanics of Biological and Bio-Inspired Materials*, ed. C. Viney, K. Katti, C. Hellmich and U. Wegst, Warrendale, PA, 2007, vol. 975E, 0975-DD06-07] and 14 percent after one week at 100 °C [D. T. Eddington, W. C. Crone and D. J. Beebe, Development of process protocols to fine tune polydimethylsiloxane material properties, *Proceedings of the Seventh International Conference on Micro Total Analysis Systems – MicroTAS 2003*, pp. 1089]. Different siloxane formulations can, however, increase its stiffness by up to one order of magnitude, as shown by Schmid and Michel [*Macromolecules*, 2000, **33**, 3042] and Whitesides and co-workers [*Langmuir*, 2002, **18**, 5314].
- 32 Certain equipment, instruments or materials are identified in this paper in order to adequately specify the experimental details. Such identification does not imply recommendation by the NIST nor does it imply the materials are necessarily the best available for the purpose.
- 33 The plot in Fig. 2(a) shows a linear relation between the wavelength and the amplitude and the exposure dose. However, the dose range explored here is deliberately biased to the production of sub-micrometre wavelengths as that is the main advantage of the plasma treatment. Extending this study to larger exposure doses has established a logarithmic dependence of the wavelength (and thus the oxidized layer thickness) with the exposure dose, providing further insight into the oxidation process itself (Cabral *et al.*, in preparation).
- 34 P.-C. Lin and S. Yang, *Appl. Phys. Lett.*, 2007, **90**, 241903.